Characterization of plasma-enhanced chemical vapor deposition carbon nanotubes by Auger electron spectroscopy

K. B. K. Teo,[a] M. Chhowalla, G. A. J. Amaratunga, and W. I. Milne
Engineering Department, University of Cambridge, Trumpington Street, Cambridge CB2 1PZ, United Kingdom

G. Pirio, P. Legagneux, F. Wyczisk, J. Olivier, and D. Pribat
Thales Research and Technology, Domaine de Corbeville, 91404 Orsay Cedex, France

(Received 20 August 2001; accepted 22 October 2001)

Plasma-enhanced chemical vapor deposition (PECVD) is a versatile technique for growing well-aligned, precisely patterned, multiwalled carbon nanotubes directly on substrates. We report on the characterization of PECVD deposited nanotubes using Auger Electron Spectroscopy (AES); we believe that this is the first comprehensive AES study of nanotubes and the effect of the deposition process on the substrate. The nanotubes contained well-crystallized graphitic carbon, in contrast to the amorphous/disordered carbon byproduct which is condensed on the substrate surface. By adjusting the deposition gas ratios, we show, using depth-profiled composition analysis, that it is possible to eliminate the unwanted amorphous carbon on the substrate surface. However, a 5 nm interfacial layer, which contained the plasma species, was always present on the substrate surface due to its exposure to the plasma. We could prevent the formation of this interfacial layer by shielding areas of the substrate from the plasma to achieve truly byproduct free deposition. This technique has allowed us to fabricate promising microelectronic field emission devices using vertically aligned carbon nanotubes. © *2002 American Vacuum Society.*
[DOI: 10.1116/1.1428281]

I. INTRODUCTION

There has been considerable progress recently in the production of vertically aligned carbon nanotubes using various forms of plasma-enhanced chemical vapor deposition (PECVD).[1–3] The PECVD technique is used in situations where high yield and uniform deposition of aligned carbon nanotubes directly on substrates is required; this cannot be achieved using other common high quality nanotube preparation techniques such as arc discharge[4] or laser ablation.[5] The PECVD process is catalytically defined, that is, nanotubes will only be nucleated wherever the catalyst is located on the substrate. Hence, ordered arrays of nanotubes and single nanotubes[3,6,7] can be precisely positioned on substrates by lithographically patterning the catalyst. This key technology will enable the application of nanotubes in various microelectronic applications such as in field emission devices.

This article reports on the characterization of PECVD deposited nanotubes using Auger Electron Spectroscopy (AES). AES was used to study the chemical composition as well as to provide qualitative information on the nature of chemical bonding present in the head and body of the nanotubes, which provided insight into the nanotube growth mechanism. Unlike nanotube growth which only occurs at catalyst sites, unwanted amorphous carbon byproducts are condensed over the rest of the substrate due to the plasma decomposition of the deposition gases. AES was used to provide depth-profiled chemical analysis of the non-nanotube areas of the substrate and to determine deposition conditions in which amorphous carbon byproducts were eliminated. More importantly, even when all the amorphous carbon was eliminated, we were still able to detect a 5 nm interfacial layer which was always present on the substrate surface due to the plasma interaction with the surface. This layer was not previously detected because energy dispersive x-ray (EDX), with less surface sensitivity compared to AES, was used.[8] As this interfacial layer could cause undesirable effects on device performance, we demonstrate how to prevent the formation of this layer on sensitive device parts by occluding/shielding them from the plasma.

[a]Corresponding author; electronic mail: kbkt2@eng.cam.ac.uk

II. EXPERIMENT

The carbon nanotubes are deposited using the PECVD of acetylene (C_2H_2) and ammonia (NH_3) gases in the presence of a nickel catalyst at 700 °C. Acetylene is the deposition gas for nanotube growth, while ammonia acts as an etching agent to suppress the deposition of amorphous carbon from the plasma decomposition of acetylene.

N-doped silicon ⟨100⟩ substrates were used in this experiment. A 2 nm nickel catalyst film and 20 nm diffusion barrier film were sputter deposited and patterned by photolithography to define the areas for nanotube growth. The diffusion barrier is necessary to prevent the diffusion of nickel into the Si substrate which occurs at temperatures above 300 °C. SiO_2 or TiN are typical diffusion barriers used for nanotube growth.[9,10]

The patterned substrates were then transferred to the deposition chamber which was evacuated to 10^{-2} Torr using a rotary pump. The substrates were heated via a tungsten resistive heater to the growth temperature of 700 °C which caused the nickel thin film to break up and agglomerate to

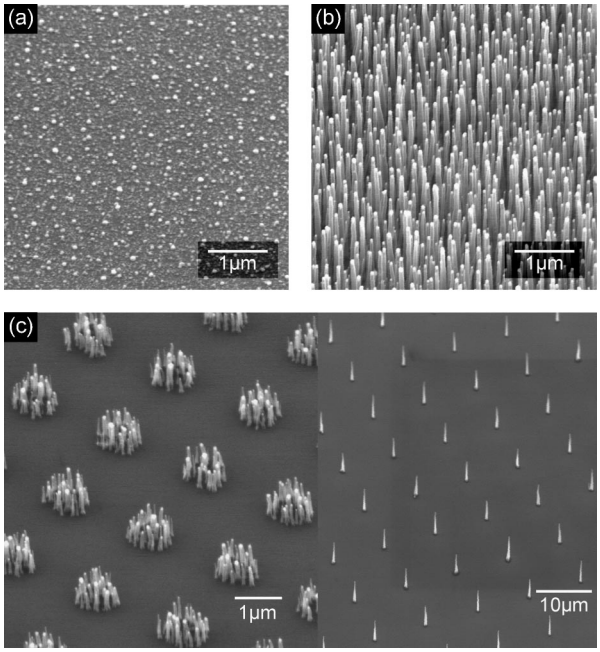

FIG. 1. (a) Nickel nanoclusters ~50 nm in diameter were formed when a thin film of nickel was annealed on a diffusion barrier at 700 °C. (b) These nickel nanoclusters catalyzed the growth of carbon nanotubes which take on the diameter of the nickel nanoclusters. (c) Selective growth of areas of nanotubes or individual nanotubes was achieved by patterning the nickel film.

form nanoclusters.[11] These nanoclusters then catalytically seed the nanotube growth [see Fig. 1(a)]. The growth was performed by introducing NH_3 and C_2H_2 into the chamber and initiating a dc plasma dicharge by applying a bias of -600 V between the heated substrates and a grounded anode 2 cm above the substrates. The nanotube deposition was performed for 15 min. This process produced ~50 nm diameter nanotubes which are $\sim 5\ \mu$m in length as shown in Fig. 1(b). Examples of selective growth of nanotubes on a substrate prepared with patterned nickel catalyst[12] is shown in Fig. 1(c).

The deposition of nanotubes by CVD is similar to the vapor–liquid–solid (VLS) mechanism[13,14] studied in the past. The carbon species dissolve and saturate in the nanocluster, and then precipitate as graphitic, tubular sheets/structures around the edges of the catalyst where the Ni thickness is least to form the nanotube.[15] If, due to a high C_2H_2 gas concentration, the expulsion of carbon proceeds at a rate higher than that required for vertical growth of the nanotube, conical graphite layers exits the particle to form a tip shape structure.[11] We believe that this conical tip shape forms because carbon diffusion occurs more rapidly around the thinner edges of the catalyst than at the center. Note that nanotip growth is only possible when the growth of the tip is faster than the growth of surface amorphous carbon which is a byproduct from high C_2H_2 gas concentrations.

The Auger analysis was carried out using a Physical Electronic PHI 680 Auger Nanoprobe with a multi-channel plate detector. The kinetic energy of the incident electron beam was 20 keV with a total current of 5 nA. Under these conditions, the electron beam diameter was typically <10 nm which allowed us to probe individual nanotubes.

TABLE I. Summary of gas flow ratios used in the experiment. The deposition time was 15 min.

C_2H_2 flow rate (sccm)	NH_3 flow rate (sccm)
30	200
40	200
50	200
60	200
100	200
150	200

In order to determine deposition conditions in which the amorphous carbon byproducts were eliminated, the C_2H_2 flow rate was varied while maintaining the same NH_3 flow at 200 sccm. The gas flow ratios used in this experiment are summarized in Table I. The non-nanotube (i.e., noncatalyzed) areas of the Si substrate were then examined using AES. The kinetic energy of the primary electron beam used was 5 keV at a current of 20 nA. Depth profiles of the substrate surfaces were obtained by sputtering the surfaces using a 2 keV Ar^+ gun.

III. RESULTS AND DISCUSSION

A. Auger analysis of carbon nanotubes

For comparison, the straight carbon nanotubes and conical nanotips of Fig. 2 were examined. These samples were tilted at 30° in order to clearly visualize the nanotubes/nanotips. Auger (*KVV*) spectra of the head and body of the nanotube and nanotip were acquired at the positions shown in the insets of Fig. 2. The differential distributions of these Auger peaks, normalized to the negative excursion of the main transition at 270 eV, are shown on Fig. 3. Qualitative insight on the bonding of the carbon atoms in the nanotube/nanotip can be obtained by line shape analysis of the Auger C (*KVV*) transition. Although the overall line shapes are rather similar and correspond to graphitic carbon, we can notice changes when we pass from the body to the head of the structures: the peak situated near 258 eV decays and becomes a shoulder.

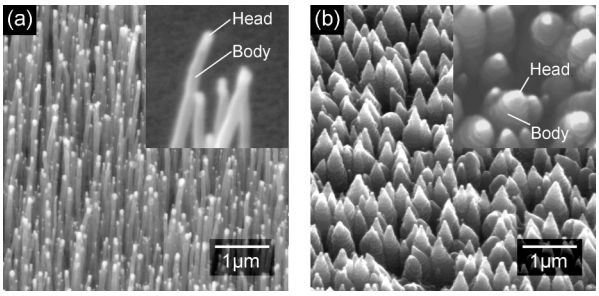

FIG. 2. (a) Straight carbon nanotubes deposited using 20% C_2H_2:NH_3 gas ratio and (b) conical nanotips deposited using 75% C_2H_2:NH_3 gas ratio. The inset shows the locations where the Auger spectra of Figs. 3 and 4 were taken.

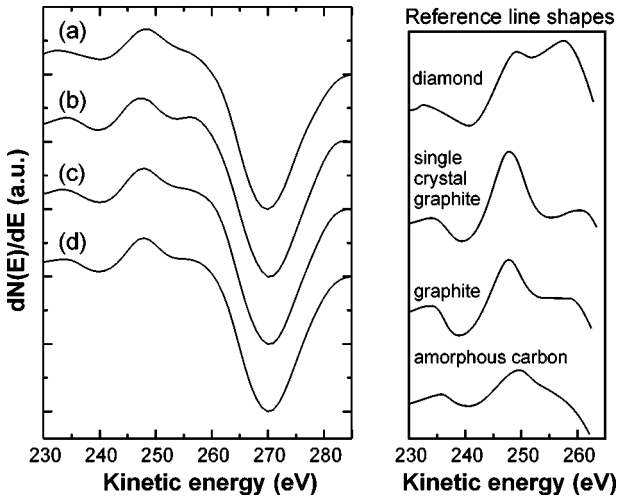

FIG. 3. Graphitic Auger C (*KVV*) peaks of (a) head of the straight nanotube, (b) body of the straight nanotube, (c) head of the conical nanotip, and (d) body of the conical nanotip. Reference line shapes of diamond, graphite and amorphous carbon are provided for comparison (Refs. 16 and 17). The better defined line shapes (240–260 eV) of the bodies of the nanostructures indicate that the bodies contained well-crystallized graphitic carbon, whereas the heads contained some disordered carbon.

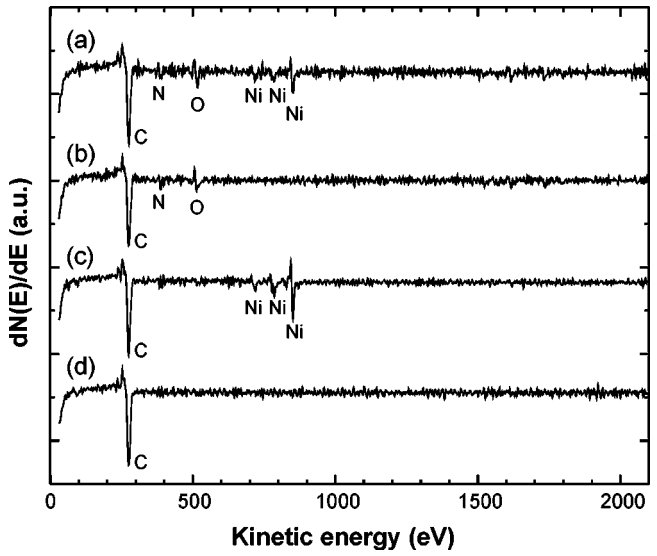

FIG. 4. Auger chemical composition analysis of (a) head of the straight nanotube, (b) body of the straight nanotube, (c) head of the conical nanotip, and (d) body of the conical nanotip.

This change is more marked in the case of the nanotube [Figs. 3(a) and 3(b)] than the nanotip [Figs. 3(c) and 3(d)].

The line shape of the *KVV* Auger peak of pure carbon depends on the valence band density of states, thus on the structural arrangement of the carbon atoms.[16] Figure 3 also shows the Auger line shape differences and more particularly, the evolutions of the two peaks at $\sim$248 eV and $\sim$258 eV, of diamond, graphite and amorphous carbon.[16] In this figure, the Auger spectrum of single crystal graphite[17] is also shown and its line shape corresponds to that of the nanotube body [Fig. 3(b)]. This indicates that the body of the nanotube contains well-crystallized sp^2-bonded carbon atoms whereas the head contains some disordered sp^2-bonded carbon atoms which cause the decrease of the peak situated at $\sim$258 eV. Disorder and defects could have been introduced into the carbon at the head of the nanotube due to the eventual existence of pentagonal structures required for the closing of the nanotubes and also severe electron bombardment/ion bombardment from energetic species in the plasma. Another possibility is that, at the termination of the deposition, the catalyst particle cooled down and the solubility of carbon in it decreased, causing the carbon to be expelled from the particle and to form disordered carbon due to the lower temperature.

A full elemental survey of the heads and bodies of the nanotube/nanotip was also obtained as shown in Fig. 4. The Ni catalyst was detected in the head of both the nanotube and the nanotip [Figs. 4(a) and 4(c)], and was responsible for the high-contrast dot seen at the head of the nanotube in all the scanning electron micrographs. The body of the nanotube and nanotip [Figs. 4(b) and 4(d)] did not contain any Ni. A further experiment at the base of the nanotubes also detected no Ni there. This indicates that all the Ni stays at the top of the nanotube during its growth: i.e., our growth mechanism is "tip-growth," in contrast to "base-growth" as observed in Ref. 2. We believe the tip-growth mechanism is favored in our process because the Ni catalyst is easily detached from the diffusion barrier layer when growth initiates.

Note that N, O, and Si atoms are also detected in only the nanotube spectra [Figs. 4(a) and 4(b)]. We believe that these signals originated from the substrate (as shown later) due to the penetration of the 20 keV electron beam through the nanotube. For the broader nanotip, the substrate contribution to the signal was minimal.

B. Auger analysis of the substrate surface

During the nanotube growth, byproducts are formed by the plasma decomposition of C_2H_2 and NH_3. If a high concentration C_2H_2 is used, amorphous carbon will be condensed on the substrate surface in areas without Ni catalyst. Conversely, if a high NH_3 concentration is used, the substrate surface would be free from amorphous carbon as it is etched away by N^+ and H^+ species in the plasma. The substrate surface was examined using deposition conditions ranging from 15%–75% C_2H_2:NH_3 in order to find conditions in which a balance was established between the deposition and etching of amorphous carbon, thus leaving the surface free from amorphous carbon. Figure 5 shows the evolution of the non-nanotube areas of the substrate under increasing C_2H_2:NH_3 ratio. For 15% [Fig. 5(a)], we observe anisotropic etching of the silicon substrate by NH_3 whereas for 75%, a thick film was found delaminating from the silicon substrate [Fig. 5(e)]. We shall only discuss the AES results for 50% C_2H_2:NH_3 and 20% C_2H_2:NH_3 in detail below as these clearly depict the cases in which amorphous carbon was or was not present on the substrate surface.

Scanning electron micrographs of samples deposited under 20% and 50% C_2H_2:NH_3 [Figs. 5(b) and 5(d)] clearly show that the 20% condition yielded an apparently clean

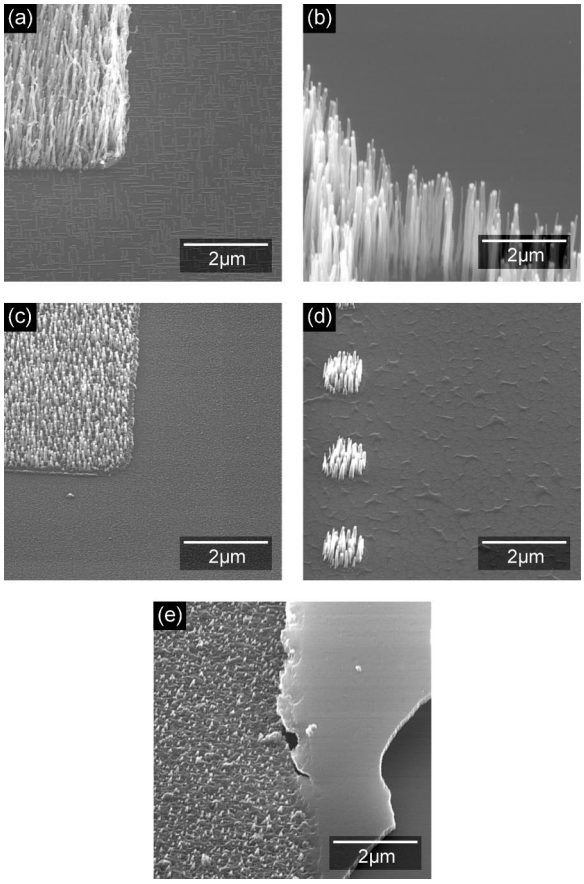

FIG. 5. Evolution of the Si substrate areas as a function of increasing $C_2H_2:NH_3$ gas ratio. (a) At 15%, the Si substrate was anisotropically etched. (b) The substrate appears ''smooth'' at 20%. (c) At 30%, byproducts began to be deposited on the substrate. (d) At 50%, there were significant byproducts on the substrate surface. (e) At 75%, a byproduct thick film was observed to delaminate from the substrate surface.

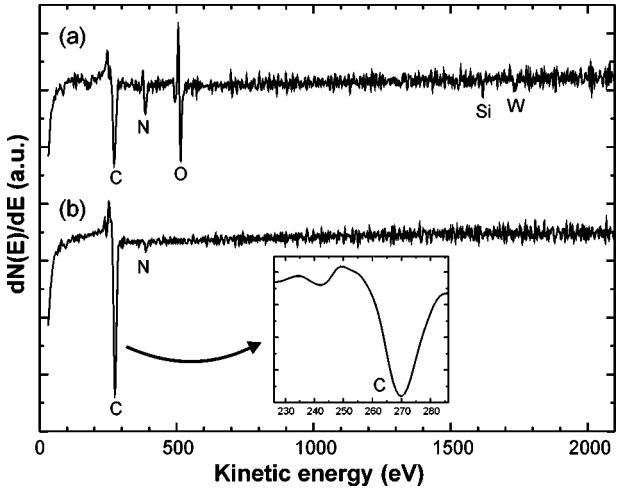

FIG. 6. Auger chemical composition analysis of the substrate surface for $C_2H_2:NH_3$ deposition gas ratios of (a) 20%, and (b) 50%. The inset plot of the Auger C (*KLL*) peak confirms that the carbon formed at 50% $C_2H_2:NH_3$ deposition gas ratio was amorphous in nature.

silicon surface on the non-nanotube areas, whereas some byproducts were condensed on the substrate for the 50% condition. A full Auger elemental survey of the noncatalyzed areas of the substrate surface was acquired as shown in Fig. 6. The ''clean'' substrate surface (for gas composition 20% $C_2H_2:NH_3$) was actually covered by a thin layer comprising C, N, O and Si atoms, and trace amount of W, whereas the condensed byproducts (for gas composition 50% $C_2H_2:NH_3$) were mainly C with a trace of N. The Auger (*KVV*) spectra in the inset of Fig. 6 indicates that the carbon was indeed amorphous and highly disordered sp^2, in contrast to the graphitic spectra obtained for the nanotube.

The composition depth-profile for 20% $C_2H_2:NH_3$ [Fig. 7(a)] showed the presence of the Si/C/N/O/W surface layer which extended a short distance into the silicon substrate. The Si (*KLL*) peak is resolvable into two contributions, namely Si-*x* (*x* for C, N, O, W) bonding for the surface layer and Si–Si bonding for the silicon substrate. The C and N atoms are products from the plasma decomposition of C_2H_2/NH_3 and they have subsequently reacted chemically with the Sii surface. The O is believed to be from the native oxide on the silicon substrate surface. The heater in our deposition system is constructed from tungsten, and so, we believe its presence on the substrate surface was due to the heater erosion by the plasma.

The composition depth-profile of Fig. 7(b) (50% $C_2H_2:NH_3$) clearly showed a thick amorphous carbon:nitrogen (*a*-C:N) layer, followed by an interfacial layer, and finally the silicon substrate. The Auger N (*KLL*) peak was resolvable into two contributions, N–C bonding in the carbon layer and N–Si bonding at the interface. The concentration of nitrogen in the interfacial layer was higher than in the carbon layer, indicating that the nitrogen species preferably reacted with the silicon surface. Nonquantitative SIMS experiments have shown that this amorphous carbon layer contains also hydrogen. A small amount of O was detected in the interface and its presence can be attributed to the native oxide on the original silicon substrate surface.

Composition depth-profile measurements of the substrate for depositions at $C_2H_2:NH_3$ gas ratios ranging from 15% to 75% are summarized in Fig. 8. The layer thicknesses presented here were determined by calibrating the sputter rate to the depth of the thickest carbon film deposited at 75% $C_2H_2:NH_3$ gas ratio (800 nm by cross-section SEM). The sputter rate for all the layers was assumed to be the same. For $C_2H_2:NH_3$ gas ratios of 30% and above, we clearly find, on top of the interface layer, an amorphous carbon layer which rapidly increases in thickness as the gas ratio increases. For amorphous carbon-free growth of nanotubes, a $C_2H_2:NH_3$ gas ratio of 20% or below must be used. A $\sim$5 nm interface layer was always present on the surface due to the exposure of the Si substrate to the C/N species in the plasma. At a gas ratio of 15%, the interface layer appeared to have extended to 10 nm. We believe that this is an artifact of the Auger measurement due to the increase of the surface roughness induced by the anisotropic etching of the silicon surface by the plasma [Fig. 5(a)].

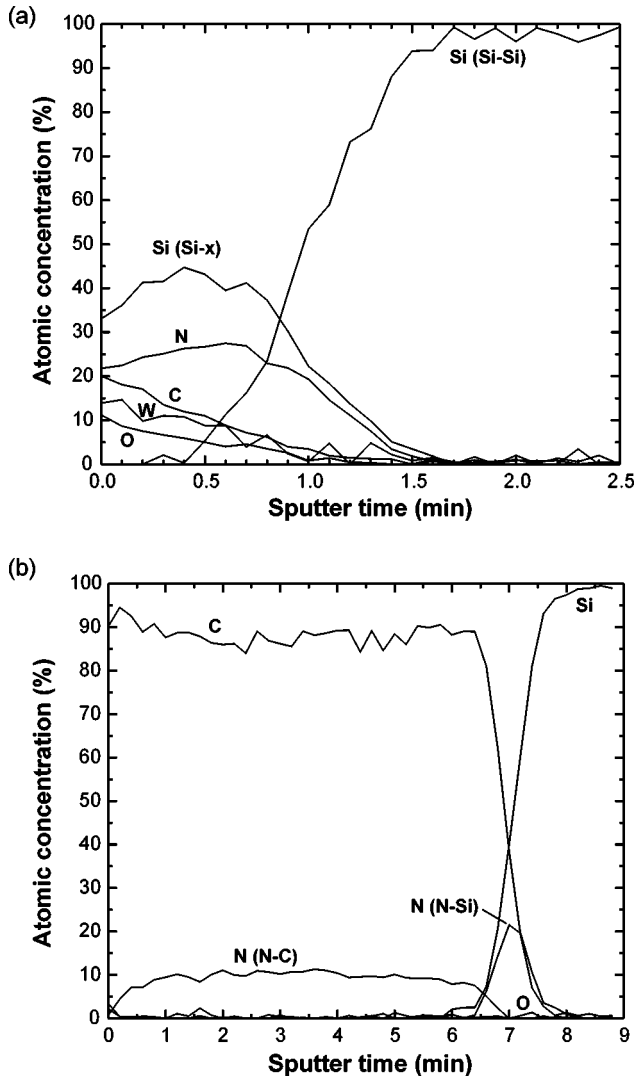

FIG. 7. Auger depth profile of the substrate surface for C_2H_2:NH_3 deposition gas ratios of (a) 20% and (b) 50%.

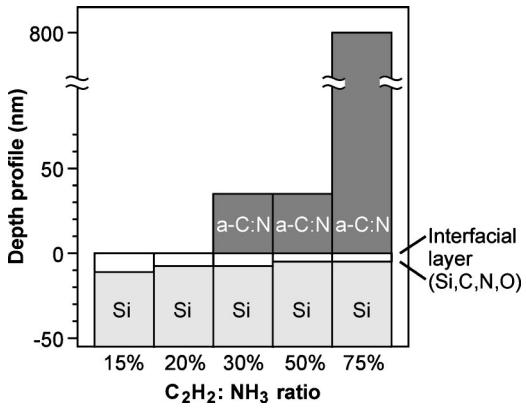

FIG. 8. Summary of depth profiles performed on the substrate surfaces of Fig. 5. For C_2H_2:NH_3 deposition gas ratios of 30% or greater, an amorphous carbon:nitrogen (*a*-C:N) film was detected on the surface of the substrate. In all cases, a thin (5–10 nm) interfacial layer was detected.

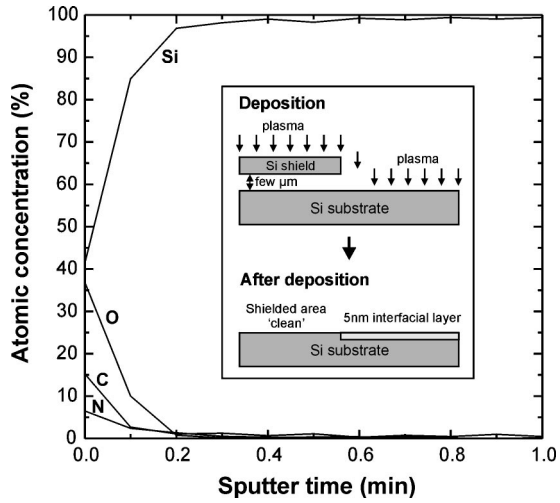

FIG. 9. Depth profile of a surface shielded from the plasma revealed that the surface was essentially unmodified (surface C/N attributed to adsorbed contaminants, O from native oxide on Si). The inset shows how the silicon shield was used to physically protect part of the substrate surface during deposition. The shield was subsequently removed for the depth-profile measurement.

C. Auger analysis of the substrate surface shielded from the plasma

It is envisaged that the interfacial layer could cause problems in device operation, such as degrading the performance of insulating layers on the substrate. To prevent its formation, it is necessary to occlude/shield the substrate from the plasma. A carbon nanotube growth was performed under the 20% C_2H_2:NH_3 gas composition (optimal for amorphous carbon-free deposition) but with part of the substrate protected from the plasma by means of a silicon mask, as shown in the inset of Fig. 9. After deposition, the mask was removed and the shielded area was examined using AES. As shown in the depth profile of Fig. 9, the substrate surface contained mainly Si and O (from native oxide on the surface) with a low amount of C and N. This C and N was rapidly sputtered away during the depth profile, which corresponded to a surface layer depth of only $\sim$1 nm. Thus, we believe that the shielded substrate surface was actually ''clean'' and the C and N were surface contaminants. The shielded surface contained no W contamination. Cleary, this shows that our silicon mask was effective in shielding the surface from the plasma.

The field emission device[18] structure of Fig. 10 is a practical demonstration of using occlusion to protect certain areas of a device from the deposition plasma. The silicon dioxide insulator was deliberately undercut beneath the polysilicon gate. The gate thus protected the sidewalls of the silicon dioxide from being coated during the plasma deposition. Vertically aligned carbon nanotubes were selectively grown *in situ* inside the device without degradation to the insulator. This functional device exhibits a peak field emission current density of 600 μA/cm^2 with 40 V gate-cathode voltage.[18]

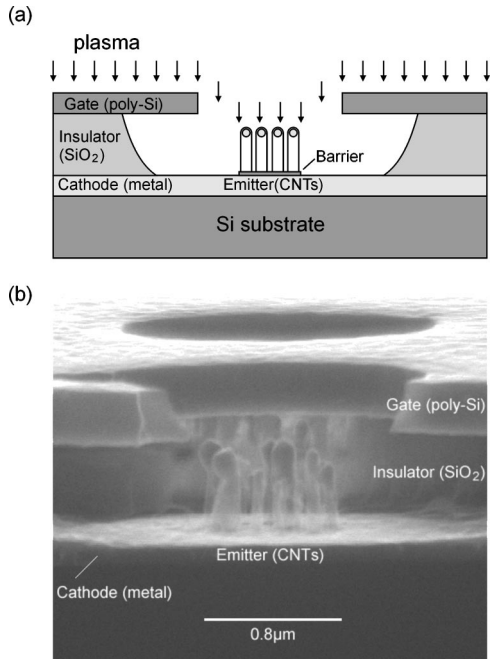

FIG. 10. Schematic of a field emission device in which the undercut insulator was shielded from plasma during carbon nanotube (CNT) deposition by the poly-Si gate above it. This prevented damage to the insulator layer which was crucial for maintaining the integrity of the insulation from gate to cathode. (b) A cross-section image of the actual field emission device showing nanotubes selectively grown inside the gated structure.

IV. CONCLUSION

The AES experiments show that carbon nanotubes deposited by PECVD are well-graphitized structures. The nanotubes grown using our process followed a tip-growth mechanism, with a high degree of crystallinity detected in the bodies and some disorder in the heads. Under 75% $C_2H_2:NH_3$ gas composition, we deposited nanotips which were still highly graphitized. This is in contrast to the noncatalyst areas of the substrate where distinctively amorphous/disordered carbon was condensed. In the best case, even when all the amorphous carbon was eliminated by using a 20% $C_2H_2:NH_3$ gas composition, a 5 nm interfacial layer still existed on the substrate surface due to the chemical reaction of the plasma species with the surface. By occluding or shielding the substrate surface, the substrate was effectively protected from the plasma and confirmed to be clean/pristine by AES. This technique provided the breakthrough which has led to the successful fabrication of field emission cathodes utilizing *in situ* growth of PECVD nanotubes.

ACKNOWLEDGMENTS

This work was partially funded by the European Commission through the IST-FET project Nanolith and VA Tech-Reyrolle U.K. K.B.K.T. acknowledges the support of the Association of Commonwealth Universities and the British Council.

[1]Z. F. Ren, Z. P. Huang, J. W. Xu, J. H. Wang, P. Bush, M. P. Siegal, and P. N. Provencio, Science **282**, 1105 (1998).
[2]C. Bower, W. Zhu, S. Jin, and O. Zhou, Appl. Phys. Lett. **77**, 830 (2000).
[3]V. I. Merkulov, D. H. Lowndes, Y. Y. Wei, G. Eres, and E. Voelkl, Appl. Phys. Lett. **76**, 3555 (2000).
[4]S. Ijima, Nature (London) **363**, 603 (1993).
[5]A. Thess, R. Lee, P. Nikolaev, H. J. Dai, P. Petit, J. Robert, C. H. Xu, Y. H. Lee, S. G. Kim, A. G. Rinzer, D. T. Colbert, G. E. Scuseria, D. Tomanek, J. E. Fischer, and R. E. Smalley, Science **273**, 483 (1996).
[6]Z. F. Ren, Z. P. Huang, D. Z. Wang, J. G. Wen, J. W. Xu, J. H. Wang, L. E. Calvet, J. Chen, J. F. Klemic, and M. A. Reed, Appl. Phys. Lett. **75**, 1086 (1999).
[7]C. Bower, O. Zhou, W. Zhu, D. J. Werder, and S. Jin, Appl. Phys. Lett. **77**, 2767 (2000).
[8]M. A. Guillorn, M. L. Simpson, G. J. Bordonaro, V. I. Merkulov, L. R. Baylor, and D. H. Lowndes, J. Vac. Sci. Technol. B **19**, 573 (2001).
[9]A. M. Rao, D. Jacques, R. C. Haddon, W. Zhu, C. Bower, and S. Jin, Appl. Phys. Lett. **76**, 3813 (2000).
[10]K. B. K. Teo, M. Chhowalla, G. A. J. Amaratunga, W. I. Milne, G. Pirio, P. Legagneux, F. Wycisk, and D. Pribat, Mater. Res. Soc. Symp. Proc. **675**, W9.1 (2001).
[11]M. Chhowalla, K. B. K. Teo, C. Ducati, N. L. Rupesinghe, G. A. J. Amaratunga, A. C. Ferrari, D. Roy, J. Robertson, and W. I. Milne, J. Appl. Phys. **90**, 5308 (2001).
[12]K. B. K. Teo, M. Chhowalla, G. A. J. Amaratunga, W. I. Milne, D. G. Hasko, G. Pirio, P. Legagneux, F. Wyczisk, and D. Pribat, Appl. Phys. Lett. **79**, 1534 (2001).
[13]R. S. Wagner and W. C. Ellis, Appl. Phys. Lett. **4**, 89 (1964).
[14]R. S. Wagner, in *Whiskers Technology*, edited by A. P. Levitt (Wiley, New York, 1970), p. 47.
[15]R. T. K. Baker, Carbon **27**, 315 (1989).
[16]P. G. Lurie and J. M. Wilson, Surf. Sci. **65**, 476 (1977).
[17]I. F. Ferguson, in *Auger Microprobe Analysis* (IOP Publishing, Bristol, 1989), p. 63.
[18]G. Pirio, P. Legagneux, D. Pribat, K. B. K. Teo, M. Chhowalla, G. A. J. Amaratunga, and W. I. Milne, Nanotechnology **13**, 1 (2002).